

Inside-Pipe Heat Transfer Coefficient Characterization of a Thermosyphon-Type Heat Pipe Suitable for the Reactor Cavity Cooling System of the Pebble Bed Modular Reactor

R. T. Dobson and I. Sittmann

Department of Mechanical Engineering, University of Stellenbosch

Private Bag X1, MATIELAND 7602, South Africa

Tel: +27 21 808 4286, Fax: +27 20 808 4958, E-mail: rtd@sun.ac.za

Abstract

The feasibility of a closed loop thermosyphon for the Reactor Cavity Cooling System of the Pebble Bed Modular Reactor has been the subject of many research projects. One of the difficulties identified by previous studies is the hypothetical inaccuracies of heat transfer coefficient correlations available in literature. This article presents the development of an inside-pipe heat transfer correlation, for both the evaporator and condenser sections, that is specific to the current design of the RCCS. A one-third-height-scale model of the RCCS was designed and manufactured using copper piping and incorporating several strategically placed sight glasses, allowing for the visual identification of two-phase flow regimes and an orifice plate to allow for forward and reverse flow measurement. Twelve experiments, lasting at least 5 hours each, were performed with data logging occurring every ten seconds. The experimental results are used to mathematically determine the experimental inside-pipe heat transfer coefficients for both the evaporator and condenser sections. The experimentally determined heat transfer coefficients are correlated by assuming that the average heat flux can be described by a functional dependence on certain fluid properties, the average heat flux is directly proportional to the heat transfer coefficient and that the heat transfer coefficient is a function of the Nusselt number. The single-phase inside-pipe heat transfer coefficients were correlated to 99% confidence intervals and with less than 30% standard deviation from experimental results. The generated correlations, along with identified and established two-phase heat transfer coefficient correlations, are used in a mathematical model, with experimental mass flow rates and temperatures used as input variables, to generate theoretical heat transfer coefficient profiles. These are compared to the experimentally determined heat transfer coefficients to show that the generated correlations accurately predict the experimentally determined inside-pipe heat transfer coefficients.

Key Words: Closed loop thermosyphons, heat transfer coefficients, two-phase flow modelling, reactor cavity cooling system, pebble bed modular reactor

1. INTRODUCTION

Passive safety systems and components are mainly incorporated into nuclear reactors to improve reliability and simplify safety systems. The IAEA notes that passive safety systems should be used wherever possible [1], keeping in mind that passivity should: reduce the number of components (reducing safety actions); eliminate short-term operator input during an accident; minimise dependence on external power sources, moving mechanical parts and

control systems, and, finally reduce lifetime-associated costs of the reactor. [2]

A closed loop thermosyphon is a reliable method of transferring thermal energy from a heat source to a heat sink, via thermally induced density gradients, resulting in natural circulation. This allows for energy transfer over relatively long distances without the use of any mechanical parts such as pumps [3]. Flow in the loop is driven by a hydrostatic pressure difference as a result of thermally

generated density gradients. One side of the loop is heated and the other cooled, thus the average density of the fluid in the heated section is less than that of the cooled section. Such thermosyphon loops find applications in the nuclear industry as cooling systems for the reactor core and surrounding structures [4].

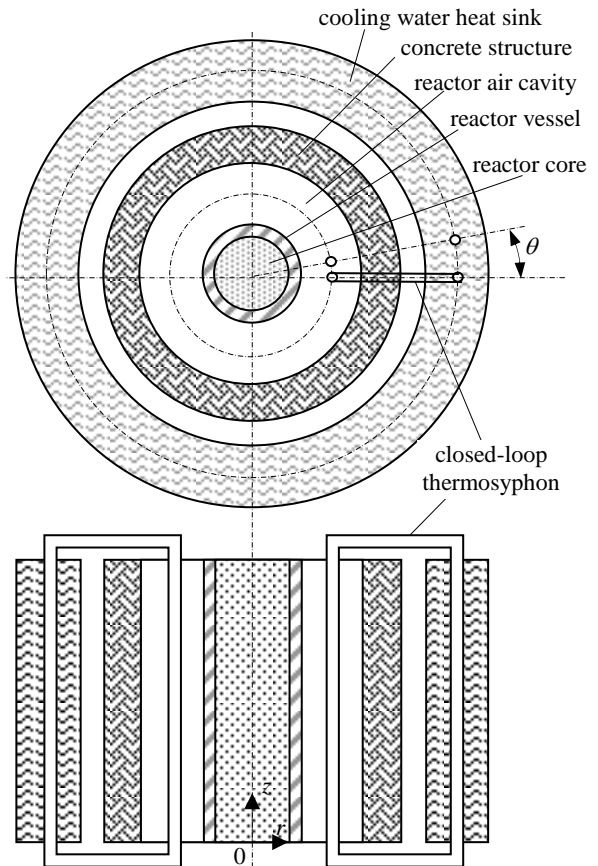
The Pebble Bed Modular Reactor (PBMR) concept evolved from a German high temperature, helium-cooled reactor design with ceramic spherical fuel elements known as INTERATOM HTR-MODUL. The main advantage of this design is that the reactor can be continuously refuelled during operation. The most noted safety feature of this design is that the silicon carbide coating of the fuel particle within the pebbles provides the first level of containment, as it keeps the fission products within itself. These design features facilitate the removal of parasitic heat through the Reactor Cavity Cooling System (RCCS).

The RCCS's primary function is to maintain the cavity temperature within a required range. This provides protection to the concrete structures surrounding the reactor and also, during loss of coolant accident operating conditions, transports parasitic heat from the reactor to the environment [5].

The current RCCS for the PBMR, as proposed by Dobson (2006), is given in Figure 1. The RCCS, in this concept, is represented by a number of axially symmetrical elements: the reactor core, reactor pressure vessel, air in the cavity between the reactor vessel and the concrete structure, the concrete structure, a heat sink situated outside the concrete structure, and a number of closed loop thermosyphons with the one vertical leg in the hot air cavity and the other leg in the heat sink. These loops are spaced around the periphery of the reactor cavity at a pitch angle θ . Vertical fins are attached to

the length of the pipe in the cavity in order to shield the concrete structure from radiation and convection (from the reactor vessel through the gap between the pipes) and to conduct the heat to the pipes [6].

Figure 1: RCCS concept (Dobson, 2006)



2. EXPERIMENTAL MODEL

A one-third-height-scale model of the RCCS was designed and manufactured. Figure 2 shows the experimental setup, the orifice plate, heat exchangers, heating elements and pressure transducers. Note that the loop is rectangular in one plane, the apparent distortion is due to the wide angle camera lens.

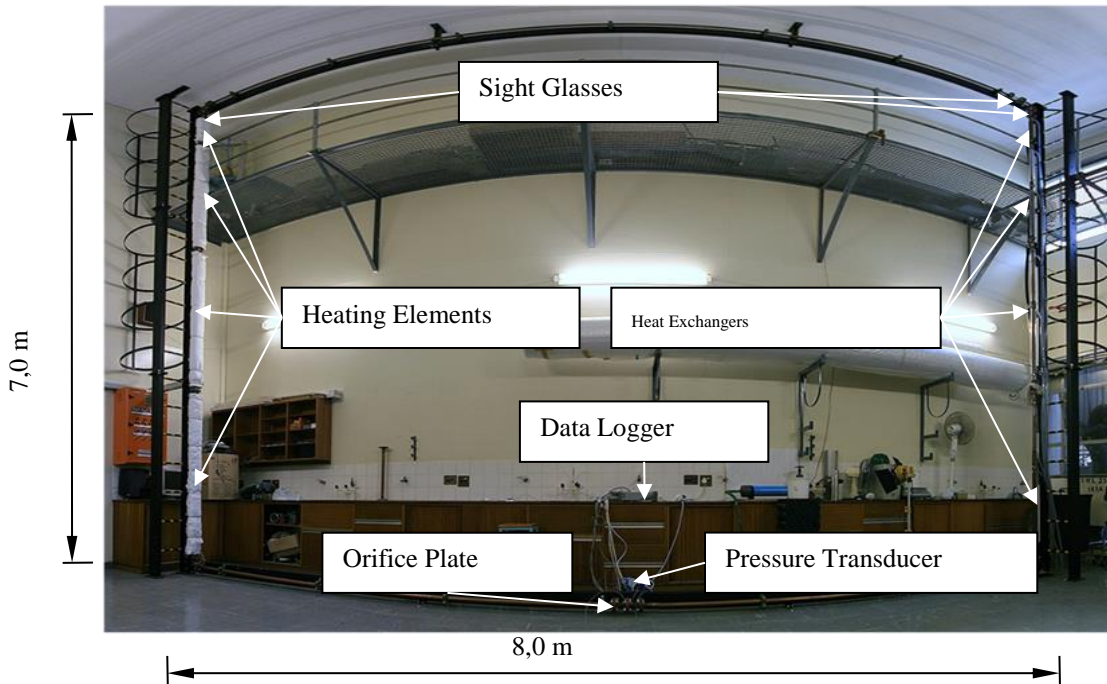


Figure 2: Experimental setup with element covers removed (taken with a wide angle lens)

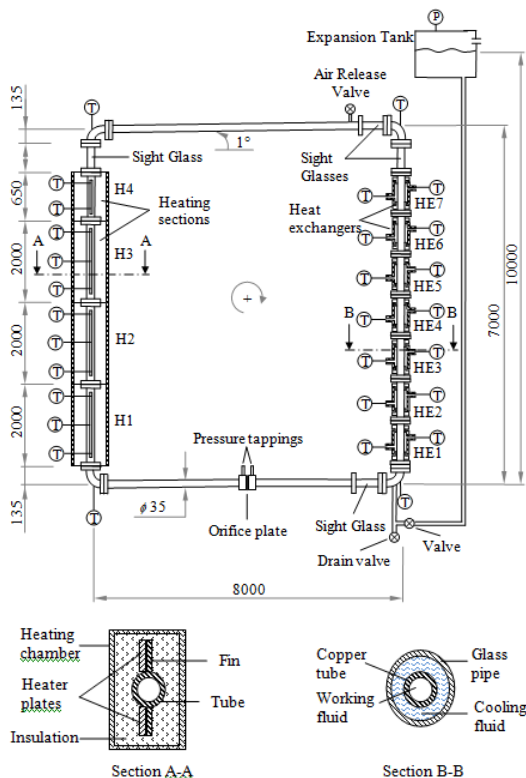


Figure 3: Thermosyphon loop

Figure 3 shows a schematic representation of the thermosyphon loop constructed for the experimental setup. The loop is constructed from 35 mm OD, 32 mm ID

copper tubes and measures 8 m wide and 7 m in height. To connect the various sections of the loop, standard 90° elbows were used and ISO 7005-3:1988 standard copper alloy flanges were designed and manufactured [7].

In previous studies, flow oscillations were identified during experimenting [8, 9]. It was therefore decided that a flow meter, capable of measuring bidirectional flow, is necessary, resulting in the design and manufacture of a British standard, unbevelled orifice plate with a β -ratio of 0.3125 [10].

The evaporator section of the thermosyphon consists of four heated sections. Three of the sections consist of a pipe, 2 m in length, onto which copper copper rectangular fins, 1.85 m in length, 50 mm wide and 10 mm thick were welded along the length. Custom made heating elements with a resistance of 35.0 Ω , each capable of providing 1500 W of heat, are attached to each fin. B64-25 Ceramic fibre (7.32 x 610 x 25 mm) insulation material surrounds the assembly. The fibre has a

density of 64 kg/m^3 and a thermal conductivity of 0.07 W/mK [11]. The fourth, and highest heating section is identical in construction to the other three except it is only 650 mm in length and the heating elements have a resistance of 105Ω , each capable of providing 500 W of heat. This gives the evaporator section a total electrical yield of 10 kW [12].

The condenser section consists of seven pipe-in-pipe heat exchangers. Six of the sections consist of a 1 m copper pipe onto which two glass outer pipes are attached using custom made copper alloy connectors and silicon O-rings yielding a total cooled length of 1.85 m . The copper alloy connector is designed with an inner groove allowing for a 2 mm diameter silicon O-ring, to ensure that a leak proof seal occurs between the connector and the copper pipe. The outside of the copper alloy connector also incorporates an O-ring groove, to ensure a leak proof seal between the connector and the glass pipe. The glass pipes have an inlet that is angled 45° to the vertical and the horizontal, ensuring that the cold water flows over the entire length of the exposed pipe, and turbulence is maintained in the cooling water in so far as possible. The fourth section, though similar in construction to the other three, consists of a 650 mm copper pipe and a 550 mm glass outer pipe.

Four transparent polycarbonate sight glasses are positioned in strategic places in order to visually identify two-phase flow patterns.

A stainless steel expansion tank was manufactured and fitted with a glass tube level indicator in order to measure the variation in tank fill level. The tank is connected to the natural circulation loop through a valve attached to the loop return line and is placed at a height of 12 m above lower horizontal section of the loop.

Twelve sheathed, K-type thermocouple probes were used to measure the working fluid temperatures at the inlet and outlet of the condenser and evaporator section of the loop as well as at the inlet and outlet of each heat exchanger. A further eleven K-type thermocouples were placed 25 mm from the tip and central to each fin in a 20 mm deep $\varnothing 1.8 \text{ mm}$ hole within the fin to measure the temperature distribution. Data integration took place over a period of 10 ms and was logged every ten seconds.

Each experiment followed the same heat input procedure. During start-up, each heating element was set to 30% of maximum power input. The working fluid temperature was monitored and the power input maintained until thermal equilibrium was reached. At that stage, the power input was increased to 50% and the process repeated. The same was done for 70% , as well as full power conditions. The power supply was then switched off and the system was allowed to cool for one hour with the cooling water running and then the water supply was switched off. The system was then left to return to initial conditions and the next experiment was only started once the loop was in thermal equilibrium with its surroundings.

3. EXPERIMENTAL HEAT TRANSFER COEFFICIENTS

The total heat added to the system can be calculated by summing the heat removed by the cooling water and the calculated heat loss:

$$\dot{Q}_{in} = \dot{Q}_{cw} + \dot{Q}_{loss} \quad (1)$$

The total heat transfer from the fins to the working fluid can also be written as:

$$\dot{Q}_{in} = A_{zod} h_{e,i} (T_{e,wall} - T_l) \quad (2)$$

Setting equation 1 equal to equation 2 and solving for h_i yields:

$$h_{e,i} = \frac{\dot{Q}_{cw} + \dot{Q}_{loss}}{A_{zod}(T_{wall} - T_l)} \quad (3)$$

Experimental results obtained were used in equation 3 to solve for the experimental inside-pipe evaporator heat transfer coefficient.

The total heat removed by the heat exchangers is calculated using the following formula:

$$\dot{Q}_{cw} = \dot{m}_{cw} C_p \Delta T_{cw} \quad (4)$$

The total heat transfer in the exchanger can also be written, using the logarithmic mean temperature method [13], as:

$$\dot{Q}_{cw} = U \phi L \Delta T_{lm} \quad (5)$$

The perimeter, ϕ , in equation need not be specified since only the overall heat transfer coefficient and perimeter product, $U \phi$, will be used in further calculations.

The logarithmic mean temperature difference (LMTD) for counter flow heat exchangers is calculated as follows [13]:

$$\Delta T_{lm} = \frac{(T_H - T_C)_L - (T_H - T_C)_0}{\ln[(T_H - T_C)_L / (T_H - T_C)_0]} \quad (6)$$

Solving for $U \phi$ yields:

$$U \phi = \frac{\dot{m}_{cw} C_p \Delta T_{cw}}{L \Delta T_{lm}} \quad (7)$$

The experimental results obtained were used in equation 7 to solve for the overall heat transfer coefficient and perimeter product. In order to isolate the inside-pipe convective heat transfer coefficient from this overall heat transfer coefficient, the heat transferred through the exchanger is analysed, taking into consideration convection from the heated water inside the copper pipe, conduction through the pipe wall and convection through the cooling water. Figure 4 shows an axially symmetric section of the heat exchanger and the corresponding thermal circuit for heat flow through the exchanger tube.

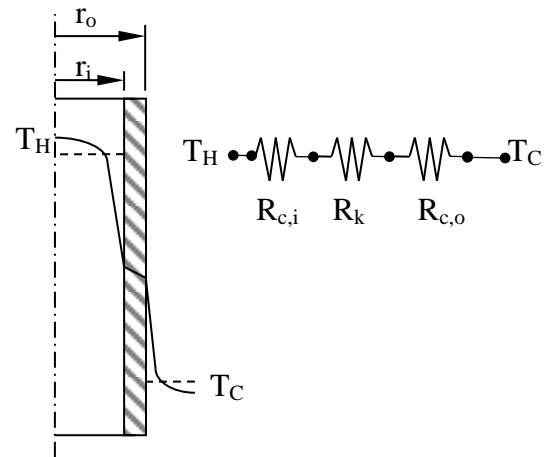


Figure 4: Local temperature profile and thermal circuit for heat flow through the exchanger tube (Mills, 1999)

By definition of the overall heat transfer coefficient [13]:

$$\frac{1}{U \phi L} = \sum R = R_{c,i} + R_k + R_{c,o} \quad (8)$$

$$\therefore \frac{1}{U \phi L} = \frac{1}{2\pi L r_i h_{c,i}} + \frac{\ln(r_o/r_i)}{2\pi k L} + \frac{1}{2\pi L r_o h_{c,o}} \quad (9)$$

The outside convective heat transfer coefficient is calculated using established correlations for forced convection. For laminar flow, a constant value is taken for the Nusselt number, and the Gnielinski correlation is used for turbulent flow [13]:

$$h_{c,o} = \frac{Nu_{cw} k_{cw}}{D_{eq}} \quad (10)$$

$$Nu_{cw} = \begin{cases} 4.861 & \text{if } Re_{cw} < 1181 \\ \frac{(f_{cw}/8) \cdot (Re_{cw} - 1000) \cdot Pr_{cw}}{1 + 12.7 \cdot (f_{cw}/8)^{0.5} \cdot (Pr_{cw}^{2/3} - 1)} & \text{if } Re_{cw} \geq 1181 \end{cases} \quad (11)$$

Isolating the inside-pipe convective heat transfer coefficient in equation 9 yields:

$$h_{c,i} = \left(2\pi r_i \left(\frac{1}{U \phi} - \frac{\ln(r_o/r_i)}{2\pi k} - \frac{1}{2\pi r_o h_{c,o}} \right) \right)^{-1} \quad (12)$$

4. CORRELATING HEAT TRANSFER COEFFICIENTS

In order to correlate the heat transfer coefficients determined from experimental data, the following assumptions are made:

- The average heat flux, \bar{q} , can be described by a functional dependence on certain fluid properties
- The average heat flux is a function of the heat transfer coefficient, in the form $\bar{q} = h_{ci}(T_w - T_b)$
- The heat transfer coefficient is a function of the Nusselt number, in the form $h = \frac{Nu_D k}{D}$

Mills (1999), suggests the following functional dependence for the average heat flux:

$$\bar{q} = f(h_{ci})$$

$$= f(Nu) = f(\Delta T, \beta, g, \rho, \mu, k, c_p, D) \quad (13)$$

Dimensional analysis of equation 13 identifies three independent dimensionless groups which characterize convective heat transfer [13]:

$$Re_q = \frac{4Q/h_{fg}}{\pi d \mu} \quad (14)$$

$$Pr = \frac{c_p \mu}{k} \quad (15)$$

$$Gr = \frac{\beta \Delta T g \rho^2 L^3}{\mu^2} \quad (16)$$

In convective heat transfer, there is a definite difference between bulk fluid and surface temperatures, creating a difficulty in selecting at which temperature the fluid properties should be calculated [13, 14]. The effect of variable properties is approximately accounted for by making use of a viscosity ratio [13]:

$$\frac{Nu}{Nu_b} = \left(\frac{\mu_s}{\mu_b}\right)^n \quad (17)$$

Where $n = -0.11$ for heating and cooling in laminar flow [13]. The Nusselt numbers for the evaporator and condenser sections can thus be evaluated by calculating a Nusselt number from bulk fluid properties and adjusting it according to equation 17.

4.1 Evaporator

The evaporator heat transfer coefficients were correlated using multi-linear regression and assuming three power-law dependencies:

$$Nu_b = a Re_q^b \quad (18)$$

$$Nu_b = a Re_q^b Pr^c \quad (19)$$

$$Nu_b = a Re_q^b Pr^c Gr^d \quad (20)$$

The dimensionless groups were averaged over 60 seconds, to decrease the oscillatory peaks, yielding 5783 separate data points to which equations 6-6 to 6-8 were correlated to 99% confidence intervals. Table 1 shows the resulting single phase regression coefficients and correlation coefficients.

Table 1: Single Phase Regression Coefficients (Evaporator)

	R^2	a	b	c	D
$Nu_b = a Re_q^b$	0.78	0.28	1.17		
$Nu_b = a Re_q^b Pr^c$	0.81	153.77	0.91	-2.81	
$Nu_b = a Re_q^b Pr^c Gr^d$	0.85	1.3×10^8	1.95	0.34	-0.835

The experimental Nusselt numbers were calculated from experimentally determined evaporator heat transfer coefficients, using equation 17. Figure 5 shows the predicted condenser Nusselt numbers (evaluated using equations 18 to 20) as a function of the experimentally determined Nusselt numbers. Figure 5(a) shows equation 18, $Nu_b = a Re_q^b$, as a function of experimental values. 56.73 % of the data falls within $\pm 35\%$ deviation levels. The average error, for this correlation is 34.92 %. Figure 5(b) shows that, using equation 19, $Nu_b = a Re_q^b Pr^c$ only 54.03 % of the data falls within $\pm 35\%$ deviation levels. The average error, for this correlation, is 34.83 %. Although the correlation coefficient is higher and the average error is lower than those obtained using equation 18, this correlation is considered a less suitable fit

because of the larger scatter in the error percentages. Figure 5(c) shows that equation 20, $Nu_b = aRe_q^b Pr^c Gr^d$, corresponds reasonably well to experimental values. 61.26 % of the data falls within $\pm 30\%$ deviation levels. The average error, for this correlation, is 31.76 %. The combination of high correlation coefficient, low average error and low error scatter make this correlation the most suitable fit.

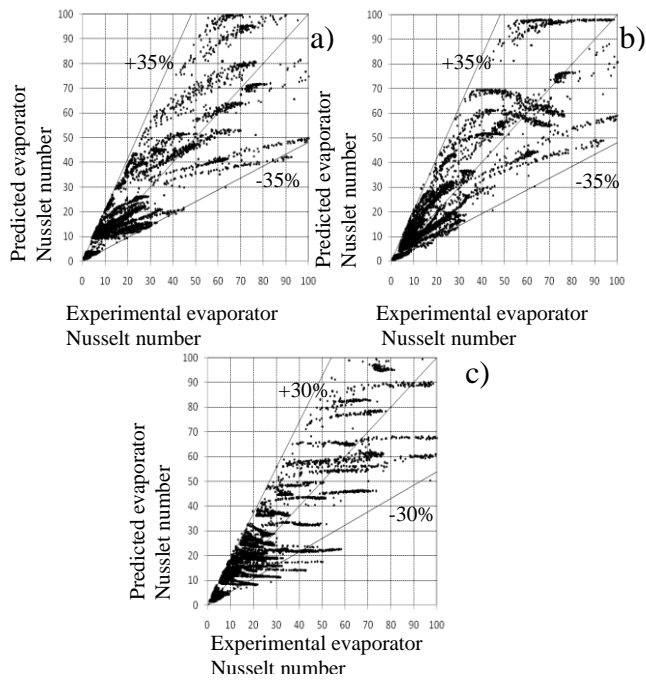


Figure 5: Predicted evaporator Nusselt number as a function of experimentally determined Nusselt numbers for single phase operating mode, equation 18 (a), equation 19 (b) and equation 20 (c)

4.2 Condenser

The dimensionless groups were averaged over 60 seconds, to decrease the oscillatory peaks, yielding 9215 separate data points to which equations 18 to 2 were correlated to 99% confidence intervals. Table -2 shows the resulting single phase regression coefficients and

correlation coefficients. Interestingly, equation 19 yields the correlation with the highest degree of variance explained.

Table 2: Single Phase Regression Coefficients (Condenser)

	R^2	a	b	c	D
$Nu_b = aRe_q^b$	0.88	5.417	0.481		
$Nu_b = aRe_q^b Pr^c$	0.90	0.579	0.538	1.094	
$Nu_b = aRe_q^b Pr^c Gr^d$	0.89	1.253	0.576	1.187	-0.042

The experimental Nusselt numbers were calculated from experimentally determined condenser heat transfer coefficients using equation 17. Figure 6 shows the predicted condenser Nusselt numbers as a function of the experimentally determined Nusselt numbers. Figure 6(a) shows that equation 18, $Nu_b = aRe_q^b$, corresponds reasonably well to experimental values. 64.23 % of the data falls within $\pm 20\%$ deviation levels and a further 17 % falls within $\pm 30\%$ deviation levels. The average error, for this correlation, is 16.95 %. Figure 6(b) shows that equation 19, $Nu_b = aRe_q^b Pr^c$, corresponds slightly better to experimental values. 64.85 % of the data falls within $\pm 20\%$ deviation levels and a further 18.15 % falls within $\pm 30\%$ deviation levels. The average error, for this correlation, is 16.95 %. Figure 6(c) shows that equation 20, $Nu_b = aRe_q^b Pr^c Gr^d$, corresponds reasonably well to experimental values. 67.16 % of the data falls within $\pm 20\%$ deviation levels and a further 17.5 % falls within $\pm 30\%$ deviation levels. The average error, for this correlation, is 16.77 %. The difference between the three correlations is negligible, the decision about which to use is thus made based on the correlation coefficient (R^2) values.

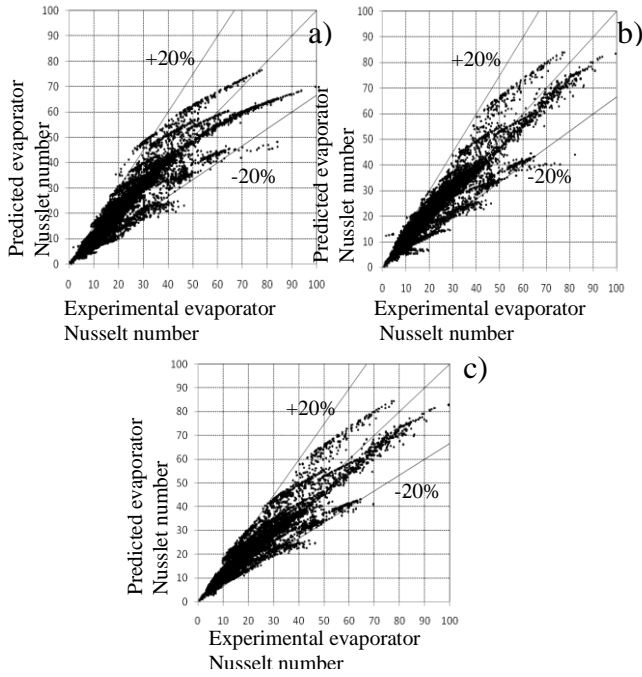


Figure 6: Predicted condenser Nusselt number as a function of experimentally determined Nusselt numbers for single phase operating mode, equation 18 (a), equation 19 (b) and equation 20 (c)

4.3 Summary

For single phase flow in the evaporator section, the power law correlation, generated using 5783 experimental data points, is used to calculate the bulk Nusselt number:

$$Nu_b = 1.3 \times 10^8 Re_q^{1.954} Pr^{0.340} Gr^{-0.835} \quad (21)$$

The average single phase Nusselt number is calculated from adjusting equation 21 using the viscosity ratio:

$$\frac{Nu}{Nu_b} = \left(\frac{\mu_s}{\mu_b} \right)^{-0.11} \quad (17)$$

The single phase inside-pipe evaporator heat transfer coefficient is then calculated using:

$$h_{e,i} = \frac{Nu k_l}{D} \quad (22)$$

For two-phase boiling, Chen's correlation [14] will be used:

$$h = h_{NB} + h_{FC} = Sh_{FZ} + Fh_l \quad (23)$$

In equation 23, h_l is the researcher's generated single phase inside-pipe

evaporator heat transfer coefficient as given by equation 21.

For single phase flow in the condenser section, the power law correlation, generated using 9215 experimental data points, will be used to calculate the bulk Nusselt number:

$$Nu_b = 0.579 Re_q^{0.538} Pr^{1.094} \quad (24)$$

The single phase inside-pipe condenser heat transfer coefficient is calculated using:

$$h_{c,i} = \frac{Nu k_l}{D} \quad (25)$$

In equation 25, Nu is the average fluid Nusselt number calculated from bulk fluid Nusselt number (equation 24) adjusted with the viscosity ratio (equation 17).

For two-phase convective condensation, the correlation proposed by Shah [15] is used:

$$\frac{h}{h_{lo}} = (1 - x)^{0.8} + \frac{3.8 \cdot x^{0.76} \cdot (1-x)^{0.04}}{Pr^{0.38}} \quad (26)$$

In equation 26, h_{lo} is the researcher's generated single phase inside-pipe condenser heat transfer coefficient (equation 24).

5. COMPARISON OF RESULTS

Experimentally obtained temperatures and mass flow rates were used as input variables in the correlations identified in the previous section. The resulting heat transfer coefficient profiles, for both the evaporator and condenser sections, are compared to experimentally determined heat transfer coefficients.

Figure 7, 8 and 9 show the inside-pipe heat transfer coefficients for the evaporator section for single phase flow operating mode with a high cooling water mass flow rate, single phase flow operating mode with a low cooling water mass flow rate and single to two-phase flow operating mode respectively.

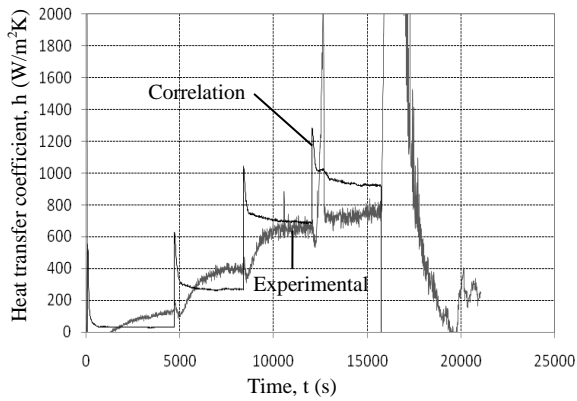


Figure 7: Comparison of inside-pipe evaporator heat transfer coefficients for single phase operating mode with high cooling water mass flow rate, for H3

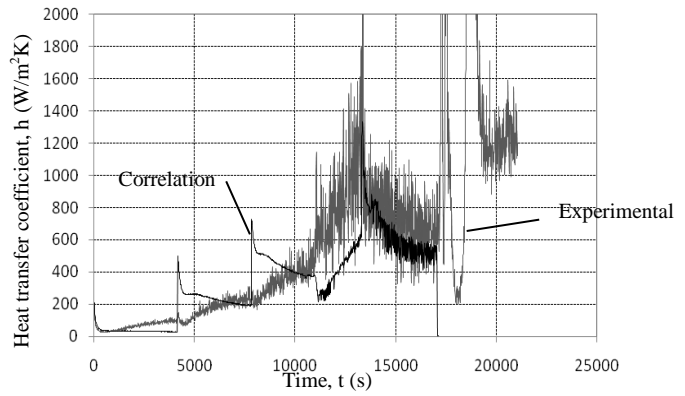


Figure 9: Comparison of inside-pipe evaporator heat transfer coefficients for single to two-phase operating mode, for H3

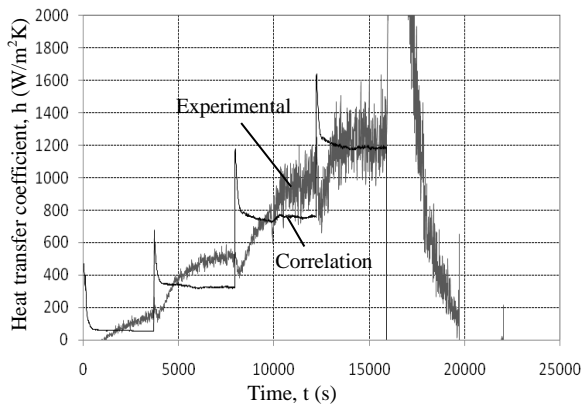


Figure 8: Comparison of inside-pipe evaporator heat transfer coefficients for single phase operating mode with low cooling water mass flow rate, for H3

The figures show that the inside-pipe evaporator heat transfer coefficient correlations, in the single phase region, rise in distinct steps corresponding to the increases in power input. Contrary to the experimental results, these steps show an initial peak in heat transfer coefficient value, which decreases steadily until a plateau is neared as the system approaches thermal equilibrium. This behaviour can be explained by the use of electrical input power, as opposed to thermal energy transferred from the heating elements to the working fluid, in the Reynolds number. Also, the effect of heat capacity was not included in the theory.

The thermal energy transferred to the working fluid increases steadily from the previous constant electrical power input level, until it approaches a plateau value equal to the current electrical power level (less minor losses to the environment) as the system reaches thermal equilibrium. This corresponds to the trend in the experimentally determined heat transfer coefficients and would thus (if used in the Reynolds number) yield a correlation which also corresponds to the same trend. Using the thermal heat transferred, in this case, is impossible as it is not measured independently and thus must be calculated using the inside-pipe evaporator heat transfer coefficient. Despite this disadvantage of the correlation, the plateau values correspond closely to those of the experimentally determined heat transfer coefficients. The single phase correlations also do not appear capture the oscillations in the heat transfer coefficient profiles.

The inside-pipe condenser heat transfer coefficient correlation depicts trends almost identical to those exhibited by the experimental data. During single phase operation, slight discrepancies in maximum values occur at high power input levels and low cooling water mass flow rates, as seen in Figure 10 and 11. After the onset of nucleate boiling in

Figure 12, the correlation oscillates with a frequency and magnitude very closely resembling the experimental values.

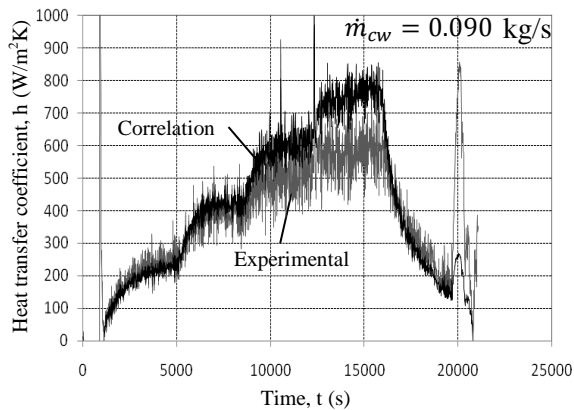


Figure 10: Comparison of inside-pipe condenser heat transfer coefficient for single phase operating mode with high cooling water mass flow rate, for HE₇,

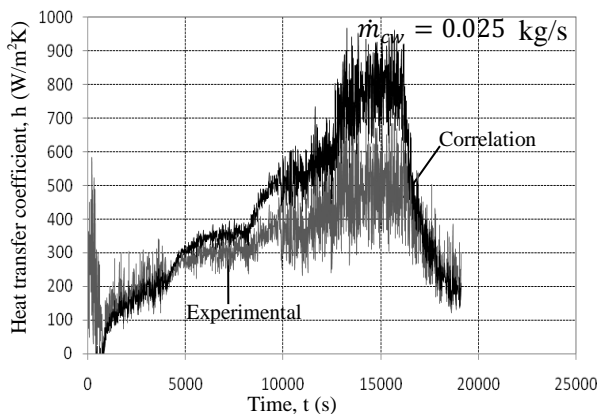


Figure 11: Comparison of inside-pipe condenser heat transfer coefficient for single phase operating mode with low cooling water mass flow rate, for HE₇

The comparisons show that the generated single phase correlations, in conjunction with established two-phase heat transfer coefficient correlations, more accurately predict inside-pipe heat transfer coefficients than single phase correlations obtained from literature.

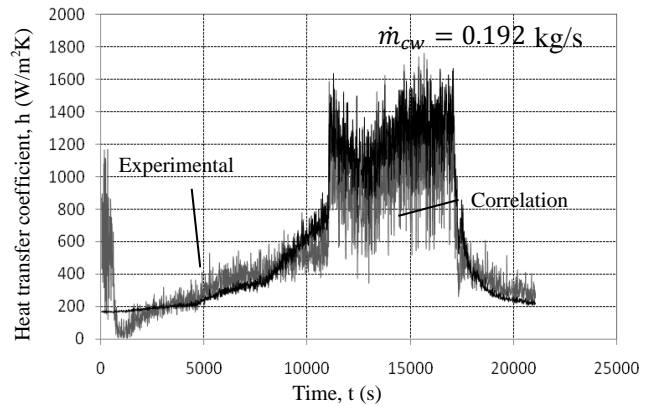


Figure 12: Comparison of inside-pipe condenser heat transfer coefficient for single to two-phase operating mode, for HE₇

6. DISCUSSIONS AND CONCLUSIONS

During single phase experimentation, start-up oscillations in the working fluid mass flow rate were identified. These oscillations, typical of natural circulation loop start-up, are caused by the working fluid buoyancy force overcoming the static friction forces and then gradually stabilize. The oscillations are considered instabilities in the system and could cause the working fluid to overheat on reactor start-up. To prevent this possibility, the reactor should be sequentially started up.

The experimental results were used to mathematically determine the experimental inside-pipe heat transfer coefficients for both the evaporator and condenser sections. Trends were identified and the general behaviour of the profiles was explained. The evaporator and condenser heat transfer coefficients follow similar trends, which is to be expected. The condenser heat transfer coefficients have slightly lower plateau values in the single phase region with a higher oscillatory amplitude. This is due to the coefficients' dependence on the cooling water temperatures which oscillate with relatively a large amplitude. This

oscillation is ascribed to the laboratory building's water supply fluctuations. In the two-phase region, where nucleate boiling is fully saturated, the condenser heat transfer coefficients are much higher than those of the evaporator section. This can be explained by the dependency of the evaporator heat transfer coefficient on the temperature difference between the tube wall and the bulk fluid. As boiling becomes saturated, this temperature difference becomes very small, resulting in a lower heat transfer coefficient value.

The heat transfer coefficients were correlated using multi-linear regression and assuming three power-law dependencies. The dimensionless groups were averaged over 60 seconds, to decrease the oscillatory peaks, yielding 5783 separate data points for the evaporator and 9215 for the condenser section. The three power-law dependencies were correlated to 99% confidence intervals yielding correlations for the single phase inside-pipe heat transfer coefficient for both the condenser and evaporator sections with an average error of less than 30% and a regression coefficients higher than 0.9.

The generated correlations, along with identified and established two-phase heat transfer coefficient correlations, were used with experimental mass flow rates and temperatures as input variables, to generate theoretical heat transfer coefficient profiles. These were compared to the experimentally determined heat transfer coefficients. The generated correlations offer a relatively accurate prediction of the experimental heat transfer coefficients. It must be noted that the generated single phase inside-pipe heat transfer coefficient correlations are only valid for the specific conditions under which they were developed i.e.: $\dot{m}_{cw,1} \leq 0.085$ kg/s, $\dot{m}_{cw,2} \leq 0.106$ kg/s, $\dot{m}_{cw,3} \leq 0.093$ kg/s, $\dot{m}_{cw,4} \leq 0.113$ kg/s, $\dot{m}_{cw,5} \leq 0.116$ kg/s, $\dot{m}_{cw,6} \leq 0.089$ kg/s, $\dot{m}_{cw,7} \leq 0.195$ kg/s, $\dot{m} \leq 14$ g/s.

If testing of the experimental system is required beyond this range, the researcher suggests that the heat transfer coefficients should be re-generated for the new conditions.

In conclusion the generated correlations can predict the single phase inside-pipe heat transfer coefficients fairly well. Although heat pipe mode was not investigated, the experimental results show that, in single phase operating mode, the experimental model can remove 7311 kW at full input power. In single to two-phase operating mode, the experimental model removes a maximum of 9306 kW. Although the single to two-phase operating mode removes more heat, the single phase operating mode is more than capable of keeping the lower leg of the thermosyphon below the specified 65 °C and there are far fewer instabilities and uncertainties associated with single phase flow. The results make a strong argument for the use of single phase natural circulation thermosyphons in the RCCS.

NOMENCLATURE

<i>A</i>	area, m ²
<i>c</i>	specific heat, J/kg K
<i>D</i>	pipe diameter, m
<i>f</i>	Darcy friction factor
<i>g</i>	gravitational constant, m/s ²
<i>Gr</i>	Grashof number
<i>h</i>	heat transfer coefficient, W/m ² K
<i>k</i>	thermal conductivity, W/m K
<i>L</i>	length, m
<i>\dot{m}</i>	mass flux, kg/s
<i>Nu</i>	Nusselt number
ϕ	perimeter, m
<i>P</i>	Pressure, Pa
<i>Pr</i>	Prandtl number
<i>q</i>	thermal energy, J
<i>R</i>	thermal resistance, K/W
<i>r</i>	radius, m
<i>Ra</i>	Rayleigh number
<i>Re</i>	Reynolds number
<i>S</i>	suppression factor

\dot{S}	heat transfer rate, W
T	temperature, K or °C
t	time, s
U	overall heat transfer coefficient, W/m ² K
V	velocity, m/s
X	Martinelli parameter
x	thermodynamic quality or mass fraction

Greek letters

α	vapour void fraction
θ	angle, rad
λ	thermal conductivity
μ	dynamic viscosity, kg/m s
ρ	density, kg/m ³
σ	surface tension, N/m
τ	shear stress, N/m ²
ϕ	fluid phase parameter
ν	kinematic viscosity, kg/ms

Subscript

a	air
b	bulk
C	cold
c	convection, condenser
cw	cooling water
D	diameter
e	evaporator
et	expansion tank
g	generated, gas
H	hot
i	inside
k	conduction
L	length
l	liquid phase
l	laminar
lm	logarithmic mean
lo	liquid only
NB	nucleate boiling
o	outside
p	constant pressure
q	thermal energy based
s	surface
sat	saturated
t	turbulent
v	constant volume
v	gaseous phase
w	water, wall
x	cross-sectional

References

1. International Atomic Energy Agency. (1996). *IAEA-TECDOC-872: Progress in design, research and development, and testing of safety systems for advanced water cooled reactors*. Vienna: IAEA.
2. International Atomic Energy Agency. (2000). *IAEA-TECDOC-1281: Natural circulation data and methods for advanced water cooled nuclear power plant designs*. Vienna: IAEA.
3. Dube, V., Akbarzadeh, A., & Andrews, J. (2004). The effect of non-condensable gases on the performance of loop thermosyphon heat exchangers. *Applied Thermal Engineering Vol 24* , 2439-2451.
4. Greif, R. (1988). Natural Circulation loops. *Journal of Heat Transfer Vol 110*, 1243-1258.
5. van Staden, M. (2001). *Analysis of effectiveness of the PBMR cavity cooling system*. South Africa: PBMR Ltd (Pty).
6. Dobson, R., and Ruppertsburg, J. (2006). Experimental evaluation of the flow and heat transfer in a closed loop thermosyphon. *JESA* .
7. ISO. (1988). *ISO 7005-3: Metallic flanges -- Part 3: Copper alloy and composite flanges*. International Organization for Standardization.
8. Ruppertsberg, J. (2007). *MScEng Thesis: Transient and scaling effects in single and two phase natural circulation thermosyphon loops suitable for the reactor cavity cooling of a pebble bed modular reactor*. University of Stellenbosch.
9. Verwey, A. (2007). *Mechanical Project 478: Passive Nuclear Reactor Cooling Using a Loop Thermosyphon*. University of Stellenbosch.
10. BSI. (1981). *BS 1042: Measurement of flow in closed conduits, Part 1: Pressure differential devices*. British Standards Institution .

11. Thermal Ceramics Pty Ltd. (n.d.). *Thermal Ceramics Product Information*. Retrieved March 2009, from Thermal Ceramics: <http://www.thermalceramics.com>
12. Loubser, J. (2008, April). Electronic Technician for Unitemp cc. johanl@unitemp.com, cell 083-225-4740
13. Mills, A. (1999). *Heat Transfer, 2nd ed.* Upper Saddle River: Prentice Hall.
14. Whalley, P. (1987). *Boiling, condensation and gas-liquid flow*. Oxford: Clarendon Press.
15. Shah, M. (1989). A general correlation for heat transfer during film condensation inside pipes. *International Journal of Heat and Mass Transfer*, Vol. 22 , 547-556.
16. Sittmann, I. (2011). *MScThesis: Inside-pipe heat transfer coefficient characterization of a loop-type heat pipe suitable for the reactor cavity cooling system of the Pebble Bed Modular Reactor*, University of Stellenbosch, Stellenbosch.